

Received January 5, 2022, accepted February 3, 2022, date of publication February 7, 2022, date of current version February 15, 2022.

Digital Object Identifier 10.1109/ACCESS.2022.3149778

# Quantitative Calibration of Three-Wavelength Road-Condition Sensor Using a Dual-Wavelength Response Ratio

SEN YANG 

College of Mechanical and Electrical Engineering, Northeast Forestry University, Harbin 150040, China

e-mail: yangsen@nefu.edu.cn

This work was supported in part by the Fundamental Research Funds for the Central Universities under Grant 2572019BF01.

**ABSTRACT** Assessing the condition of a road exposed to the atmosphere is crucial for safety. A three-wavelength road-condition sensor is a noncontact sensor that can be used for qualitative recognition and quantitative measurement of road conditions. However, the sensor is not robust to anomalous changes in the light intensity received that can be caused by several factors (such as changes in distance to the measuring point from a road bump or pothole). These changes cause the measurement state to deviate from the calibration state, reducing the sensor detection accuracy. However, existing studies on reducing the influence of the abovementioned problems on road-condition detection have only focused on how to ensure robustness in the qualitative classification of road-covering types, and no studies have been performed on how to ensure robustness in the quantitative measurement of the road-covering thickness. Thus, a quantitative calibration method for three-wavelength road-condition sensors using a dual-wavelength response ratio is proposed in this study. This method consists of using the response voltage ratio of two wavelengths to replace the response voltage of one wavelength during the quantitative calibration of sensors, making quantitative measurement insensitive to the deviation between measurement and calibration states. Comparison experiments were performed using the three-wavelength road-condition sensor calibrated by different quantitative methods, and an analysis was performed on the influence of the deviation of the measurement state from the calibration state on the quantitative measurement results and the measured covering thickness under changes in the measurement state. The experimental results verified the effectiveness of the novel approach compared with the traditional quantitative calibration method.


**INDEX TERMS** Dual wavelength, quantitative calibration, response ratio, road condition sensor, robustness.

## I. INTRODUCTION

Assessing the condition of a road exposed to the atmosphere is crucial for safety [1]. Various techniques to classify road conditions have been developed, including those based on changes in the electrical resistance [2], machine vision [3], [4], infrared thermometry [5], and diffuse reflection in the near-infrared range [6], [7]. The operating principle of a three-wavelength road-condition sensor (TRCS) is the active transmission of an infrared light beam on the road surface and detection of the backscattered signal at three selected wavelengths. Casselgren *et al.* detected changes in the depths of water and ice road cover and classified different

types of ice by utilizing polarized shortwave infrared light and a sensor consisting of three laser diodes with wavelengths of 980 nm, 1310 nm, and 1550 nm [8]. Jonsson classified dry, wet, snowy, and icy road conditions using a sensor consisting of three IR detectors with peak sensitivities at 960 nm, 1550 nm, and 1950 nm [9]. Ruiz-Llata *et al.* developed a road-condition sensor based on diffuse reflectance spectroscopy in the near-infrared region using semiconductor laser diodes with wavelengths of 1460 nm, 1490 nm, and 1550 nm [10].

A TRCS needs to be robust to changes in intensity that can be caused by several factors (such as changes in the distance to the measuring point due to bumps and shocks [11], [12]). These changes cause the measurement state to deviate from the calibration state, resulting in a measured voltage that is anomalous compared to the calibration voltage. Existing

The associate editor coordinating the review of this manuscript and approving it for publication was Ajit Khosla .

studies that have been conducted to address this problem have focused on how to improve the robustness of qualitative classification by the sensor to road-covering types [8], [10]. One solution is to assume that the intensity changes due to bumps and shocks are the same for all detection wavelengths. That is, the shape of the spectra remains the same and only the intensities of the peaks change, such that the ratio of the two wavelengths involved is insensitive to changes in the intensity [13]. This method enables the calculation of an intensity-independent parameter that only changes with the road condition. Similar concepts and solutions have been used in other research schemes [14].

The abovementioned problems impact quantitative measurement of the thickness of a road surface covering more severely than qualitative classification. However, there is a lack of research on how to ensure the stability of quantitative measurement of the thickness of a road surface covering under the influence of the abovementioned problems. To address this issue, a method based on a dual-wavelength response ratio (DRRB) is proposed in this study for quantitative TRCS calibration that improves the sensor robustness over that of the conventional single-wavelength response-based (SRB) quantitative calibration method. A parameter, the dual-wavelength response ratio, is introduced into the quantitative fitting procedure that depends on the thickness of the road surface covering and not the light intensity, thus reducing adverse effects resulting from the deviation between the measurement and the calibration states on the measured thickness.

This paper is structured as follows. In Section II, the TRCS and calibration methods are described. The TRCS calibration results are presented in Section III Subsection A, and the influence of the deviation between the measurement and calibration states on the quantitative measurement results is analyzed in Section III Subsection B. An analysis of the change in the measured covering thickness with the measurement state is performed in Section III Subsection C.

## II. METHODS AND PRINCIPLES

### A. THE COMPONENTS OF A TRCS

A three-wavelength road-condition sensor was developed. The sensor classifies road conditions as dry, wet, snowy, and icy. Based on the variance of the wavelength ratios for the four aforementioned types of surfaces [12], the sensing wavelengths used in this study were 940 nm, 1310 nm, and 1550 nm. Fig. 1 shows a simplified schematic of the TRCS.

As shown in Fig. 1, the TRCS consists of an optical system, three laser diodes, a modulated signal generator, an optical switch, a detector, an I/V converter, a preamplifier, a relay, a lock-in amplifier, an A/D converter, an SCM module, a GPRS module, and a cloud platform. The optical system is used for the emission and reception of light. An InGaAs detector with a waveband from 800 to 1700 nm is used in conjunction with a lock-in amplifier for phase-sensitive detection. Finally, a DC voltage signal proportional to the

incident light is transmitted to the cloud platform and processed using a LabView program.

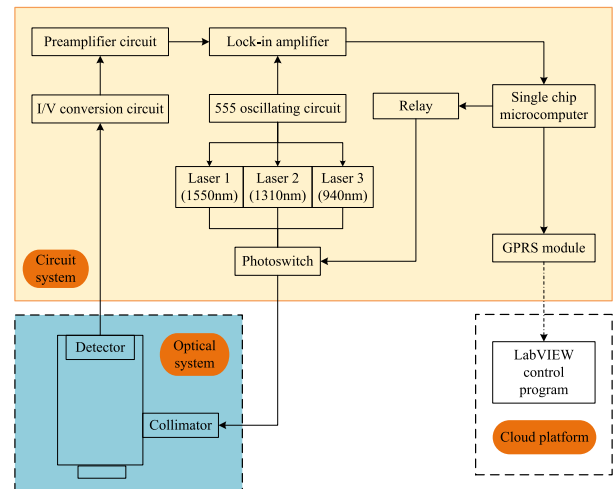


FIGURE 1. A simplified schematic of the TRCS.

### B. THE PRINCIPLES OF THE DIFFERENT CALIBRATION METHODS

There are two TRCS calibration methods, which differ in terms of the independent variable used for quantitative fitting: (1) SRB and (2) DRRB. Fig. 2 shows the calibration and measurement procedures of the two quantitative calibration methods.

#### 1) SRB METHOD

The SRB calibration function can be obtained through polynomial approximation as follows:

$$D_{ss} = \sum_{i=0}^n a_i V_{ss\lambda}^i \quad (1)$$

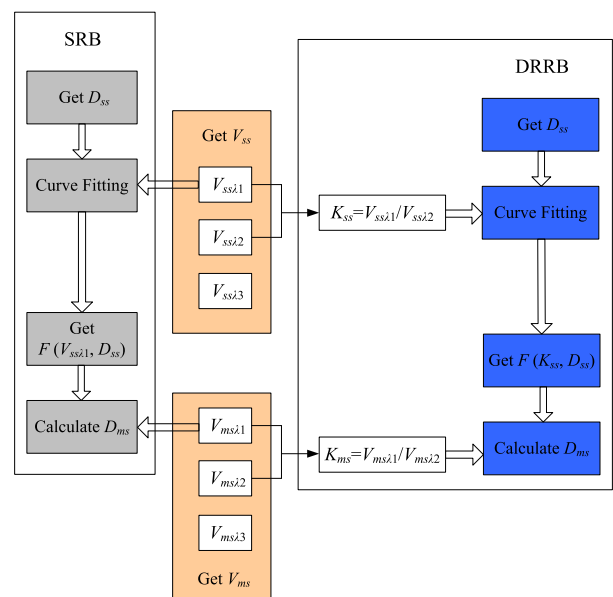


FIGURE 2. Calibration and measurement procedures for two quantitative calibration methods.

where  $D_{ss}$  is the thickness of a standard sample;  $V_{ss\lambda_1}$  is the response voltage at a wavelength  $\lambda_1$ ;  $a_i$  is a coefficient determined by the least-squares method; and  $n$  is determined by the calibration data.

The road condition is identified by using Equation (1) in conjunction with the measurement voltage  $V_{ms}$ , where the thickness  $D_{ms}$  of a measurement sample can be obtained by Equation (2).

$$D_{ms} = \sum_{i=0}^n a_i V_{ms\lambda_1} \quad (2)$$

2) DRRB METHOD

In DRRB calibration, the influence of changes in the measurement state is reduced by selecting the independent variable for the fitting function as the calibration parameter  $K_{ss}$ , which is defined by the following equation:

$$K_{ss} = V_{ss\lambda_1} / V_{ss\lambda_2} \quad (3)$$

The  $D_{ss}$  of the standard sample is obtained using the calibration function as follows:

$$D_{ss} = \sum_{i=0}^n a_i K_{ss} \quad (4)$$

The measurement parameter  $K_{ms}$  for the road-condition measurement can be obtained by Equation (5).

$$K_{ms} = V_{ms\lambda_1} / V_{ms\lambda_2} \quad (5)$$

The thickness  $D_{ms}$  of a measured sample can be determined using Equation (6).

$$D_{ms} = \sum_{i=0}^n a_i K_{ms} \quad (6)$$

III. EXPERIMENTS

A. TRCS CALIBRATION

Fig. 3 shows images of the TRCS and standard samples. Different artificial road coverings were used as standard samples for TRCS calibration. Calibration wavelengths of 940 nm and 1310 nm were used in the DRRB method. The calibration distance was 150 mm, and the calibration angle was 90°. In this study, the road-covering thickness and calibration distance were measured by a digital display Vernier caliper (BK-318, BiaoKang) and digimatic micrometer (0-25 mm and 25-50 mm, SHSIWI), and the calibration angle was measured by an angle ruler with a digital display (JDC-200, BiaoKang).

Fig. 4 shows the TRCS calibration data obtained at 940 nm and 1310 nm, respectively, where I, W and S represent icy, wet and snowy road conditions, respectively. The relationship between the covering thickness and response voltage was obtained using polynomial fitting.

The TRCS was calibrated as follows.

(1) Measure the covering thicknesses  $D_{ss}$  of standard samples.

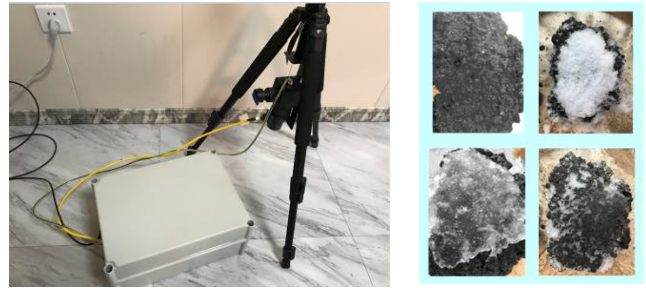


FIGURE 3. Images of the TRCS and standard samples.

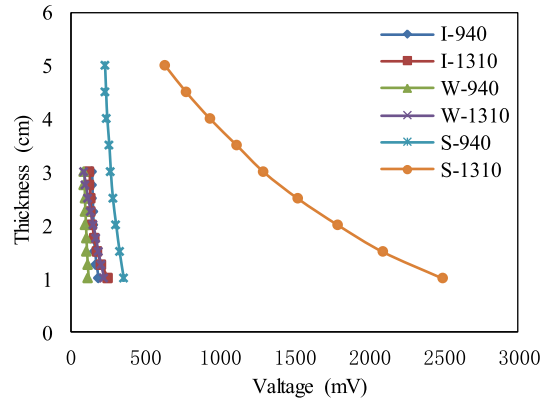


FIGURE 4. TRCS calibration data.

- (2) Measure the response voltages  $V_{ss}$  at three wavelengths using the TRCS.
- (3) Calculate the calibration parameters  $K_{ss}$ .
- (4) Obtain the relationship between  $V_{ss}$  or  $K_{ss}$  and  $D_{ss}$  by data fitting.
- (5) Update the measurement program.

B. THE INFLUENCE OF THE DEVIATION BETWEEN THE MEASUREMENT AND CALIBRATION STATES ON QUANTITATIVE MEASUREMENT

In this section, the influence of deviations between the measurement and calibration states on quantitative measurement is analyzed. First, the calibrated voltage is artificially increased to varying extents to simulate different degrees of deviation between the measured and calibrated states. Then, the artificially changed calibrated voltage (that is, the voltage measured after the measurement state has changed) was input into the calibration equation to obtain the measured thickness (that is, the thickness measured after the measurement state has changed). Finally, the measurement error resulting from the deviation between the measurement and calibration states was obtained by comparing the measured thickness with the calibrated thickness (that is, the normal measured thickness).

The experimental process is detailed below.

(1) Obtain the calibration functions  $F_1(V_{ss940}, D_{ss})$ ,  $F_2(V_{ss1310}, D_{ss})$ , and  $F_3(V_{ss940/1310}, D_{ss})$  using the calibration data presented in Fig. 4.

(2) Increase  $V_{ss}$  by 1% and 5% and calculate  $D'_{ss}$  using the calibration functions obtained in (1).

(3) Calculate the root-mean-squared error (RMSE) based on Equation (7).

$$RMSE = \sqrt{\frac{1}{n} \sum_{i=1}^n (D'_{ss} - D_{ss})^2} \quad (7)$$

(4) Evaluate the performance of different quantitative calibration methods under different deviations of the measurement state from the calibration state.

A polynomial order of 3 was obtained by the least-squares fit. Three road-covering types were measured: ice, water, and snow. The RMSEs obtained for different quantitative calibration methods and road coverings are shown in Fig. 5.

As shown in Fig. 5, the  $RMSE_{DRRB}$ s were smaller than the  $RMSE_{SRB}$ s, indicating that the DRRB method can reduce the quantitative measurement error resulting from the deviation between measurement and calibration states. The  $RMSE_{SRB}$ s for the 5% voltage change were higher than the  $RMSE_{SRB}$ s for the 1% voltage change, whereas the  $RMSE_{DRRB}$ s were equal for 1% and 5% voltage changes, such that the deviation between the  $RMSE_{DRRB}$  and  $RMSE_{SRB}$  increases

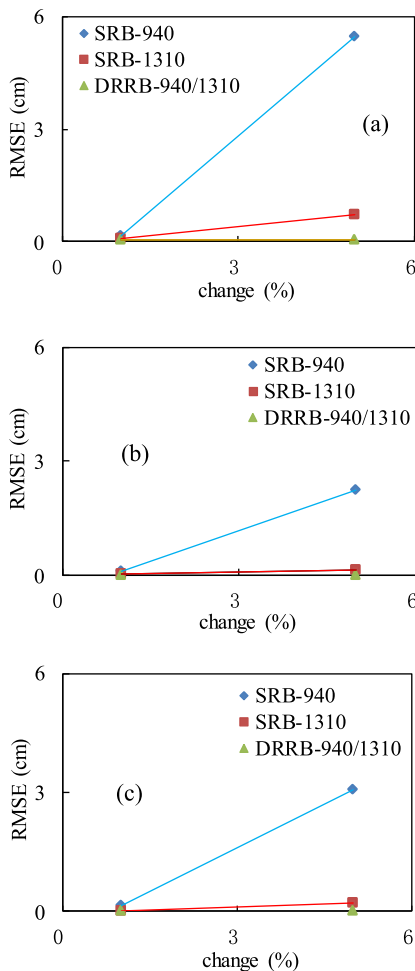


FIGURE 5. RMSE based on calibration data using different methods for road coverings of (a) ice; (b) water; and (c) snow.

with the magnitude of the voltage change. Thus, we infer that the DRRB method is more effective than SRB for large deviations between calibration and measurement states. The  $RMSE_{SRB-940}$ s were higher than the  $RMSE_{SRB-1310}$ s, indicating that the SRB performance depended on the selected wavelength. Among the different covering types, the  $RMSE_{water}$  was smallest, followed by  $RMSE_{snow}$ , and  $RMSE_{ice}$  was the largest. We speculated that the thickness and voltage errors resulting from the irregular shape of the ice sample caused the largest measurement errors to be obtained for ice coverings, whereas the accuracy of the thickness measurement of the water sample resulted in a better data distribution and minimized the measurement error for water coverings.

However, the experimental results in Fig. 5 were affected by measurement and fitting error. To compare the calibration methods more accurately, an additional comparative analysis was performed using  $y = f(x)$  for the simulated calibration data. The simulated calibration data used for this comparison are shown in Fig. 6.

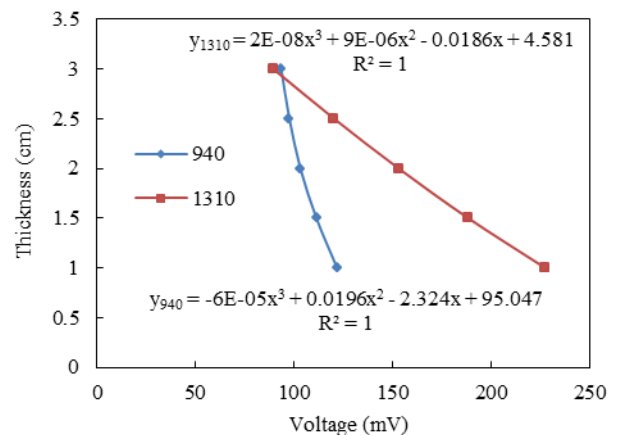


FIGURE 6. The simulated calibration data.

The same comparison procedures were used as described for Fig. 5. The thickness value  $y$  was set to be 1 cm, 1.5 cm, 2 cm, 2.5 cm, and 3 cm. The voltage  $x$  was calculated using  $y_{940}$  and  $y_{1310}$ . The calibration parameter  $k$  for the DRRB method was calculated from  $x_{940}/x_{1310}$ . In this comparative analysis, the voltage  $x$  was changed by  $-10\%$  and  $10\%$  to simulate deviations in different directions between the calibration and measurement states, corresponding to road conditions such as road bumps and potholes. The RMSEs for the simulated calibration data are shown in Fig. 7.

There is no measurement error in the simulated calibration data  $y = f(x)$ , and fitting error is only present for DRRB-940/1310. As shown in Fig. 7, the  $RMSE_{DRRB}$  was  $2.78E-4$ , that is, for an approximately ideal state, the DRRB method can almost eliminate the quantitative measurement error caused by the difference in calibration and measurement states. The  $RMSE_{DRRB}$ s were smaller than the  $RMSE_{SRB-1310}$ s and considerably smaller than the  $RMSE_{SRB-940}$ s, again demonstrating the superiority of the

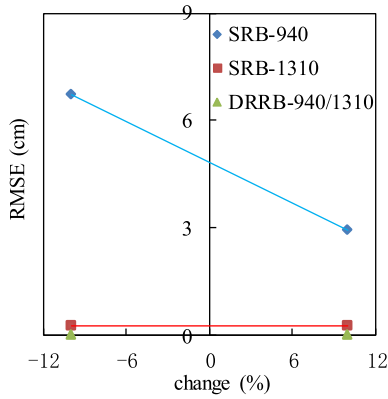


FIGURE 7. The RMSEs obtained for the comparative analysis based on simulated calibration data.

DRRB method. For voltage changes of  $-10\%$  and  $10\%$ , the  $RMSE_{SRB-1310}$ s were approximately equal, whereas the  $RMSE_{SRB-940}$ s were different. This result is concluded to result from the different distributions of the analog data for the two wavelengths.

**C. COMPARISON EXPERIMENT FOR MEASURING THE COVERING THICKNESS BASED ON A CHANGE IN THE MEASUREMENT STATE**

In this subsection, the TRCS calibrated using the SRB and DRRB methods was applied to the quantitative measurement of the covering thickness. Considering sensor operability and the similarity of the comparison results for RC-I, RC-W, and RC-S, water was selected as the road covering to be measured. The measurement distances were set from 13.8 cm to 16.2 cm, which were different from the calibration distance (150 mm). Fig. 8 shows the setup used to measure the covering thickness under a change in the measurement state.

In Fig. 8,  $l_c$  is the calibration distance,  $l_m$  is the measurement distance, and  $x_i$  is the deviation between the measurement and the calibration distances. The measured voltages for different measurement distances are shown in Table 1.

In Table 1, the measured distance is different from the calibrated distance, showing that the measured state deviates from the calibrated state. Comparing the data in Figure 4 and Table 1 shows that for the same measured covering thickness, the difference between the measured and calibrated distances

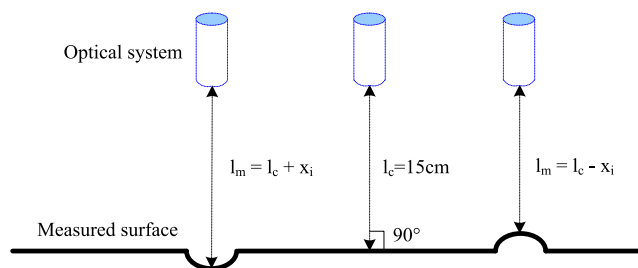


FIGURE 8. The setup used to measure the covering thickness under a change in the measurement state.

TABLE 1. Measured voltages for different measurement distances.

Water thickness (cm)	Measurement distance (cm)	Measurement voltage (mV)	
		940 nm	1310 nm
1	14.0	125.783	232.081
	16.0	117.901	223.805
2	13.8	112.289	162.932
	16.2	95.431	143.513
3	13.8	101.304	93.411
	15.9	91.697	88.938

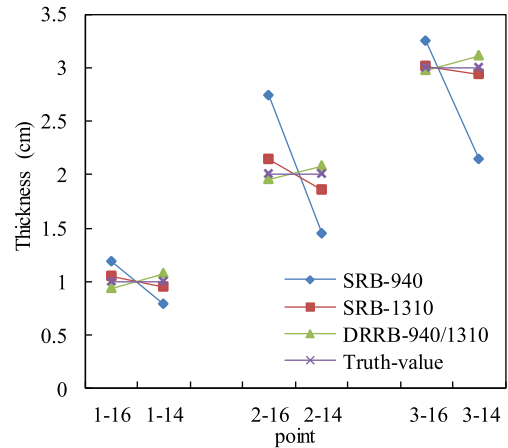


FIGURE 9. Measured thickness using different calibration methods under changes in the measurement state.

TABLE 2. RMSEs for different calibration methods under changes in the measurement state.

	SRB-940	SRB-1310	DRRB-940/1310
RMSE (cm)	1.727	0.051	0.032

results in different radiation levels received by the sensor and therefore, different measured and calibrated voltages.

Fig. 9 shows the measured thickness for different calibration methods under changes in the measurement state. In the abscissa of Fig. 9, 1, 2, and 3 correspond to the truth-values of the covering thickness, and 14 and 16 correspond to the measurement distances.

In Fig. 9, for each covering thickness, the slope of the line between the measuring points at the two measuring distances reflects the influence of the deviation in the measurement state from the calibration state. When the measurement distance deviated from the calibration distance, the thicknesses measured using DRRB were closer to the truth-values than those measured using SRB. Using the SRB method, the thicknesses measured at 940 nm were closer to the truth-values than those measured at 1310 nm. The experimental results validate the superiority of the DRRB method over the SRB calibration method for improving the robustness of the sensor for quantitative measurement.

To accurately assess the performance of the different calibration methods, the RMSEs were calculated based on Equation (7) and the data in Fig. 9. The RMSEs for different calibration methods under changes in the measurement state are shown in Table 2. When the measurement distance deviated from the calibration distance, 35.3% lower RMSEs were obtained using the DRRB method than by using the SRB method.

#### IV. CONCLUSION

A DRRB quantitative calibration method was proposed in this study to improve the robustness of the TRCS for quantitative measurement. In this novel method, the introduction of a dual-wavelength response ratio into the quantitative fitting process reduces adverse effects resulting from the deviation between the measurement and calibration states on the measured thickness. Comparison experiments were performed on TRCS. The comparative results validated that the DRRB method reduces the quantitative measurement error resulting from the deviation between measurement and calibration states.

#### REFERENCES

- [1] L. Hu, X. Zhou, X. Zhang, F. Wang, Q. Li, and W. Wu, "A review on key challenges in intelligent vehicles: Safety and driver-oriented features," *IET Intell. Transp. Syst.*, pp. 1093–1105, Jun. 2021, doi: [10.1049/itr2.12088](https://doi.org/10.1049/itr2.12088).
- [2] H. Tabatabai and M. Aljuboori, "A novel concrete-based sensor for detection of ice and water on roads and bridges," *Sensors*, vol. 17, no. 12, p. 2912, Dec. 2017, doi: [10.3390/s17122912](https://doi.org/10.3390/s17122912).
- [3] P. Jonsson, J. Casselgren, and B. Thornberg, "Road surface status classification using spectral analysis of NIR camera images," *IEEE Sensors J.*, vol. 15, no. 3, pp. 1641–1656, Oct. 2015, doi: [10.1109/JSEN.2014.2364854](https://doi.org/10.1109/JSEN.2014.2364854).
- [4] J. Casselgren, S. Rosendahl, M. Sjö Dahl, and P. Jonsson, "Road condition analysis using NIR illumination and compensating for surrounding light," *Opt. Lasers Eng.*, vol. 77, pp. 175–182, Feb. 2016, doi: [10.1016/j.optlaseng.2015.08.002](https://doi.org/10.1016/j.optlaseng.2015.08.002).
- [5] M. Riehm, T. Gustavsson, J. Bogren, and P. E. Jansson, "Ice formation detection on road surfaces using infrared thermometry," *Cold Regions Sci. Technol.*, vol. 83, pp. 83–84, Dec. 2012, doi: [10.1016/j.coldregions.2012.06.004](https://doi.org/10.1016/j.coldregions.2012.06.004).
- [6] L. Colace, F. Santoni, and G. Assanto, "A near-infrared optoelectronic approach to detection of road conditions," *Opt. Laser Eng.*, vol. 51, pp. 633–667, May 2013, doi: [10.1016/j.optlaseng.2013.01.003](https://doi.org/10.1016/j.optlaseng.2013.01.003).
- [7] A. Piccardi and L. Colace, "Optical detection of dangerous road conditions," *Sensors*, vol. 19, pp. 1360–1367, Jan. 2019, doi: [10.3390/s19061360](https://doi.org/10.3390/s19061360).
- [8] J. Casselgren, M. Sjö Dahl, and J. P. Leblanc, "Model-based winter road classification," *Int. J. Vehicle Syst. Model. Test.*, vol. 7, no. 3, pp. 268–284, 2012, doi: [10.1504/IJVSMT.2012.048941](https://doi.org/10.1504/IJVSMT.2012.048941).
- [9] P. Jonsson, "Remote sensor for winter road surface status detection," in *Proc. IEEE Sensors*, Oct. 2011, pp. 1285–1288, doi: [10.1109/ICSENS.2011.6127089](https://doi.org/10.1109/ICSENS.2011.6127089).
- [10] M. Ruiz-Llata, M. Rodriguez-Cortina, P. Martin-Mateos, O. E. Bonilla-Manrique, and J. R. Lopez-Fernandez, "LiDAR design for road condition measurement ahead of a moving vehicle," in *Proc. IEEE Sensors*, Oct. 2017, pp. 1–3, doi: [10.1109/ICSENS.2017.8234230](https://doi.org/10.1109/ICSENS.2017.8234230).
- [11] J. Casselgren, M. Sjö Dahl, and J. Leblanc, "Angular spectral response from covered asphalt," *Appl. Opt.*, vol. 46, no. 20, pp. 4277–4288, 2007, doi: [10.1364/AO.46.004277](https://doi.org/10.1364/AO.46.004277).
- [12] R. Du, G. Qiu, K. Gao, L. Hu, and L. Liu, "Abnormal road surface recognition based on smartphone acceleration sensor," *Sensors*, vol. 20, no. 2, p. 451, Jan. 2020, doi: [10.3390/s20020451](https://doi.org/10.3390/s20020451).
- [13] J. Casselgren, M. Sjö Dahl, M. Sanfridsson, S. Woxneryd, J. Valldorf, and W. Gessner, "Classification of road conditions—to improve safety," *Adv. Microsystems Automotive Appl.*, vol. 2007, pp. 47–59, Aug. 2007, doi: [10.1007/978-3-540-71325-8\\_4](https://doi.org/10.1007/978-3-540-71325-8_4).
- [14] C. Gong, Q. Wu, H. Zhang, R. Wang, K. Xiong, Y. Okabe, and F. Yu, "Dual-frequency acousto-ultrasonic sensing of impact damage in composites for mitigating signal instability," *Struct. Health Monit.*, Mar. 2021. [Online]. Available: <https://journals.sagepub.com/doi/10.1177/1475921721996625>, doi: [10.1177/1475921721996625](https://doi.org/10.1177/1475921721996625).



**SEN YANG** received the M.S. and Ph.D. degrees in instrument science and technology from the Harbin Institute of Technology, China, in 2011 and 2018, respectively. He is currently a Lecturer with the College of Mechanical and Electrical Engineering, Northeast Forestry University, China. His research interests include road condition detection, infrared radiation measurement, and automatic control.

...